ASSOCIAZIONE NAZIONALE ITALIANA DI
INGEGNERIA SISMICA
ANIDIS
Italian National Association of Earthquake Engineering

XVIII CONVEGNO ANIDIS
L'ingegneria sismica in Italia
ASCOLI PICENO 2019
15-19 Settembre

Synergetic application of Seismic Interferometry and Operational Modal Analysis for comprehensive SHM of historic structures

Enrique García-Macías[a], Filippo Ubertini[a]

[a] *Department of Civil and Environmental Engineering, University of Perugia, Perugia, Italy*

Keywords: Damage identification; Historic buildings; Structural health monitoring; Wave propagation.

ABSTRACT

This paper proposes the use of monitoring systems based upon the coupled application of Operational Modal Analysis and Ambient Noise Deconvolution Interferometry for the Structural Health Monitoring of historic structures. The potential of this approach is exemplified through three different case studies of Italian historic masonry structures, namely the Sciri Tower in Perugia, the Consoli Palace in Gubbio, and the bell-tower of the Basilica of San Pietro in Perugia. The first case study represents a typical example of a masonry tower incorporated into a building aggregate, and illustrates the application of the proposed approach for continuous system identification. The second one regards a particular case of a monumental masonry palace with limited separation between the sensors and complex wave propagation. Finally, the last case study illustrates the synergetic application of Operational Modal Analysis and Ambient Noise Interferometry for earthquake-induced damage detection.

1   INTRODUCTION

Historic structures constitute very sensible elements of tangible heritage, encompassing manifold resources of cultural identity, architectural and artistic assets, as well as an important source of economic income. The growing awareness about the importance of their conservation has fostered the implementation of numerous Structural Health Monitoring (SHM) systems, specially through dynamic measurements and Operational Modal Analysis (OMA) (Masciotta et al. 2017). Such systems allow the condition-based maintenance and decision making of rehabilitation through the continuous assessment of the modal features of the structure. These techniques are particularly well-suited for historic structures since the monitoring is performed under operational conditions with minimal impact on the structure. Nevertheless, while effective for the assessment of the global behaviour of structures, these techniques may fail at detecting local pathologies with limited effects on the modal features of the system. In this light, Seismic Interferometry

poses a complementary technique for non-parametric damage identification with superior capability for detection of local damage. This approach conceives the dynamic response of structures as a superposition of propagating waves, and evaluates the condition of the structure through the velocity of travelling pulses between pairs of sensors (Todorovska and Trifunac 2008). Given that the propagation of elastic waves is directly related to the local stiffness of the structure, the presence of damage between pairs of sensors can be inferred through local wave delays in a fully data-driven way. Although some successful applications have been reported in the realm of reinforced-concrete structures, works regarding the application of Seismic Interferometry to ambient vibrations in historic structures are practically nonexistent.

In this context, this work proposes the use of monitoring systems based upon the coupled application of OMA and Ambient Noise Deconvolution Interferometry (ANDI) for the SHM of historic buildings. In particular, the potential of this approach is exemplified through three different case studies of Italian historic masonry structures, namely the Sciri Tower in

Perugia, the Consoli Palace in Gubbio, and the bell-tower of the Basilica of San Pietro in Perugia. The first case study represents a typical example of a masonry tower incorporated into a building aggregate, and presents some results on the synergetic application of OMA and ANDI for the continuous system identification of the tower during three weeks. The second case study regards a particular case of a monumental masonry palace with limited separation between the sensors. Finally, the third case study illustrates the application of the proposed approach for earthquake-induced damage identification. To do so, two different ambient vibration tests (AVTs) conducted before and after the 2016 Central Italy seismic sequence are studied. The results demonstrate that, while damage can be detected by both OMA and ANDI in the shape of resonant frequency shifts and global wave delays, respectively, the analysis of local wave delays additionally allows the localization and, to some extent, the quantification of damage.

2   THEORETICAL BACKGROUND: DECONVOLUTION INTERFEROMETRY

Let us consider a masonry building equipped with an array of sensors monitoring its response $u(z,t)$ along the height $0 < z < H$, where t is the time variable and H the total height (see Fig. 1). Assuming the structure as a linear time-invariant system, the records of a reference sensor $u(z_{\text{ref}},t)$ and of an arbitrary one $u(z,t)$ can be related in time as (Şafak 1999):

$$u(z,t) = u(z_{ref},t) * h(z,z_{ref},t) =$$
$$\int_0^t u(z_{ref},t) * h(z,z_{ref},t-s)\,\mathrm{d}s, \tag{1}$$

Or, alternatively, in the frequency domain ω as:

$$\hat{u}(z,\omega) = \hat{u}(z_{ref},\omega)\hat{h}(z,z_{ref},\omega), \tag{2}$$

where * indicates convolution, and a hat indicates Fourier transform. Functions $\hat{h}(z,z_{ref},\omega)$ and $h(z,z_{ref},t)$ denote the transfer function (TF) and the impulse response function (IRF) between the output and the input signals, respectively. The IRFs can be computed by taking the inverse Fourier transform of the corresponding TFs in a finite frequency band $\omega \le \omega_{\max} = (f_s/2)/(2\pi)$, with f_s being the sampling frequency, as:

$$h(z,z_{ref},t) = \frac{1}{2\pi}\int_{-\omega_{\max}}^{+\omega_{\max}} \hat{h}(z,z_{ref},t)\,\mathrm{e}^{-\mathrm{i}\omega t}\mathrm{d}\omega. \tag{3}$$

In addition, a regularized version of the TFs in Eq. (3) is usually introduced to avoid numerical instability due to division by null numbers as (Snieder and Şafak 2006):

$$h(z,z_{ref},t) \approx \frac{1}{2\pi}\int_{-\omega_{\max}}^{+\omega_{\max}} \frac{\hat{u}(z,\omega)\overline{\hat{u}(z,\omega)}}{|\hat{u}(z,\omega)|^2 + \eta}\,\mathrm{e}^{-\mathrm{i}\omega t}\mathrm{d}\omega, \tag{4}$$

where the bar indicates complex conjugate, and η denotes a regularization parameter. In this work, we use $\eta = 0.1P$, with P being the mean amplitude spectral power.

The velocity of the propagating pulses can be computed by peak-picking analysis of the IRFs as sketched in Fig. 1. To do so, the time lag τ_i between the motions at levels z_{i+1} and z_i is obtained by picking the maxima of the IRFs along a ray path, and the velocity is computed as $v_i = l_i/\tau_i$, with $l_i = z_{i+1} - z_i$.

It is usually necessary to filter the waveforms to a certain frequency band. To do so, a band-pass filter $\hat{S}$ can be applied to the TFs in the frequency domain as:

$$\hat{S}(\omega,\omega_1,\omega_2) = \begin{cases} 1 & \omega_1 \le |\omega| \le \omega_2 \\ 0 & \text{otherwise} \end{cases}, \tag{5}$$

with ω_1 and ω_2 denoting the cut-off frequencies.

Finally, the extension of this formulation to the continuous monitoring of structures is essential for the identification (detection, localization and
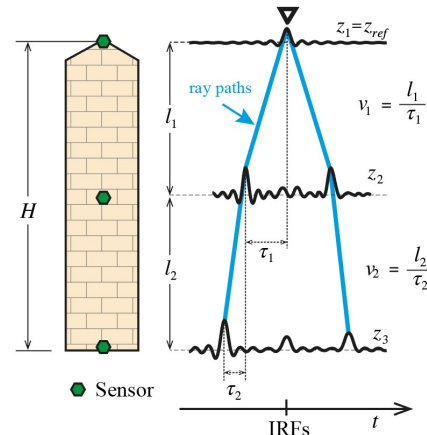

Figure 1. Schematic of the peak-picking analysis of a waveform obtained by deconvolution interferometry considering a virtual source at the roof level.

quantification) of early-stage damage. To this aim, deconvolution can be applied to ambient-vibration records considering N time windows with a certain overlap to minimize the variance of the estimated wave velocities. Afterwards, the waveforms can be stacked (averaged) over the intervals as follows (Nakata and Snieder 2013):

$$h(z,z_{ref},t) \approx \frac{1}{N} \sum_{n=1}^{N} \left(\frac{1}{2\pi} \int_{-\omega_{max}}^{+\omega_{max}} \frac{\hat{u}(z,\omega)\overline{\hat{u}(z,\omega)}}{|\hat{u}(z,\omega)|^2 + \eta} e^{-i\omega t} d\omega \right)$$

(6)

3 CASE STUDY I: THE SCIRI TOWER

The first case study is the 41 m high masonry tower named Torre degli Sciri located in the historical centre of Perugia in Italy (see Fig. 2(a)). The Sciri Tower dates back to the 13th century and, nowadays, it is the only remaining medieval tower in a good state of preservation in the city. The tower has a hollow rectangular cross-section of 7.15 × 7.35 m, and it is inserted in a building ensemble with approximate plan dimensions of 21.8 × 24.6 m. Three façades of the tower are connected to the adjoining buildings up to a height of 17 m, while the fourth one remains exposed.

With the aim of simultaneously identifying the modal features and wave propagation properties of the tower, a continuous AVT was performed for three weeks, since February 13th until March 10th 2019. To this end, 12 high sensitivity (10 V/g) uniaxial PCB 393B12 accelerometers were installed at four levels of the tower, namely $z = 40.5$ m, $z = 33.5$ m, $z = 24.0$ m and $z = 8.4$ m (see Fig. 2(b)), as well two K-type thermocouples at the level $z = 40.5$ m (indoor and outdoor). Ambient vibrations were recorded at two different sampling frequencies to evaluate
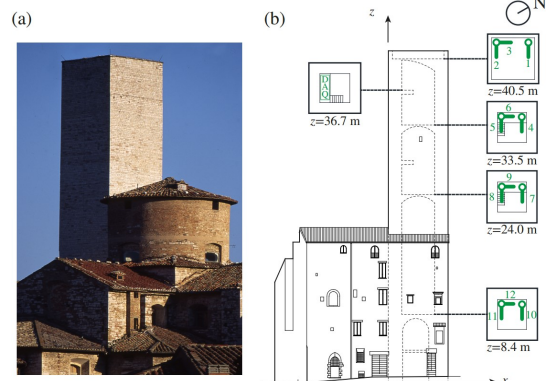

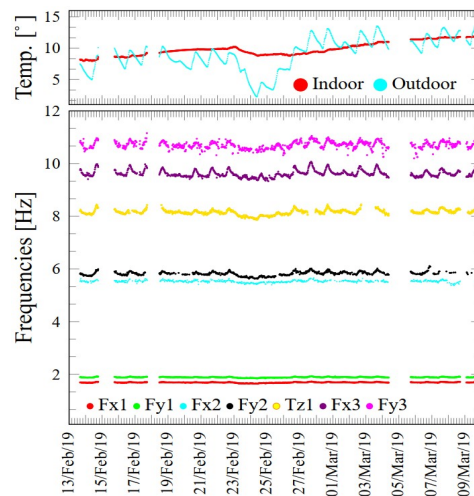Figure 2. View of the Sciri Tower (a), and sketch of the structural monitoring system (b).

Figure 3. Temperature time series and frequency tracking in the Sciri Tower since February 13th until March 10th 2019.
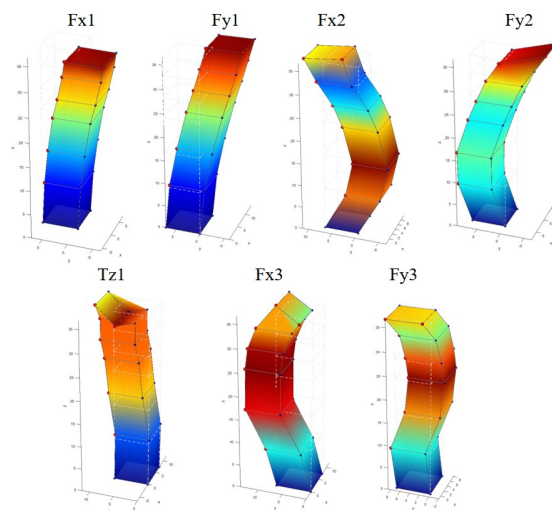

Figure 4. Experimentally identified mode shapes of the Sciri Tower estimated through COV-SSI on February 13th 2019 at 14:00 UTC.

the robustness of the wave identification, including 200 Hz and 5000 Hz. Field data were acquired using a multi-channel data acquisition system (DAQ) model NI CompactDAQ-9184 located at level $z = 36.7$ m, and data were stored in separate files containing 30-min long time series.

The modal features of the tower have been automatically identified using the Covariance driven Stochastic Subspace Identification (COV-SSI) method. To do so, every 30-min long acceleration records have been downsampled to 200 Hz, and the modal features have been extracted by an in-house modal identification code implemented in MATLAB. Seven vibration modes have been identified in the frequency range between 0 and 12 Hz as shown in Fig 3, including two flexural modes in the NW direction (Fx1 and Fx2), two flexural modes in the SW

Table 1. Experimentally identified natural frequencies f_i, and damping ratios ς_i estimated through COV-SSI on 13th February 2019 at 14:00 UTC.

Mode	f_i [Hz]	ς_i [%]
Fx1	1.69	0.88
Fy1	1.89	0.78
Fx2	5.45	4.66
Fy2	5.86	1.92
Tz1	8.15	2.18
Fx3	9.82	1.03
Fy3	10.84	3.88
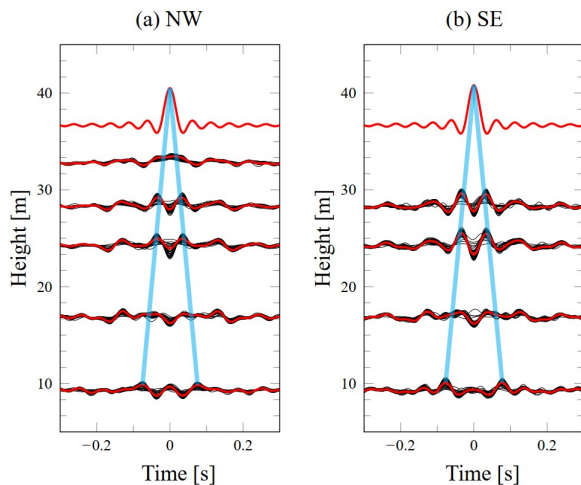
Figure 5. Staking waveforms over 30-min intervals of the IRFs for the first 48 hours and filtered in broad-band frequency of 0.1-20 Hz, (a) NW component, and (b) SE component. The red lines indicate the staked IRFs over the first 48 hours (f_s=200 Hz).

direction (Fy1 and Fy2), one torsional mode (Tz1), and two higher order flexural modes, (Fx3 and Fy3). The corresponding mode shapes are plotted in Fig. 4, and their natural frequencies and damping ratios are reported in Table 1.

In order to continuously assess the propagating waves in the tower, ANDI has been applied to 10-min-long ambient vibration records considering a stacking time of 30 min with 50% overlap. In addition, virtual sources have been considered at the roof level (z_{ref} = 40.5 m), and the waveforms have been filtered to the frequency band 0.1-20 Hz. Figure 5 shows the IRFs in the NW and SE directions obtained for every 30-min-long acceleration records during the first 48 hours and a sampling frequency of f_s=200 Hz. For each deconvolved waveform, the arrival times of the travelling pulses have been automatically detected and tracked. Figure 6 shows the computed travel times versus the distance from the reference level z_{ref} on the basis of the results previously shown in Fig. 5. The error bars in the graph represent the standard deviation of the computed arrival times from the waveforms in

Fig. 5, and the global velocities (velocity of the waves to cross the whole tower, representing the black dashed lines in Fig. 6) are computed by the peak-picking analysis of the waveforms resulting from the staking of the waves throughout the first 48 hours. Shear S-wave velocities of 359.71 m/s and 360.03 m/s are obtained for the NW and SE directions, being slightly higher in the latter one where the contribution of the building aggregate is larger.

Figure 7 shows the time histories of the identified wave velocities considering two layers (L1 (9.3 m<z<28.4 m), and L2 (28.4 m<z<36.7 m)) and the whole tower, for sampling frequencies of 200 Hz and 5000 Hz. It is noted in this figure that the wave velocity is larger in the bottom layer, where the contribution of the building aggregate is localized. It is also noted that the sampling frequency of 200 Hz fails to identify the temperature fluctuations, and many outliers are present stemming from poor sampling-induced limitations in the peak-picking analysis. Conversely, the larger sampling frequency of 5000 Hz makes it possible to obtain clear day/night fluctuations. In this case, it is observed that there is a positive correlation with temperature, that is, increasing temperatures during the daytime yields increasing wave velocities, while decreasing temperatures during the night-time leads to decreasing wave velocities. A similar behaviour can be also found in Fig. 3 in terms of resonant frequencies, and it indicates that the stiffness of the tower increases with temperature. Such an effect is common in masonry structures, where the thermal expansion of masonry originates the closure of superficial cracks or micro-cracks, as well as minor discontinuities. Finally, it is also observed that the temperature sensitivity is larger in the bottom
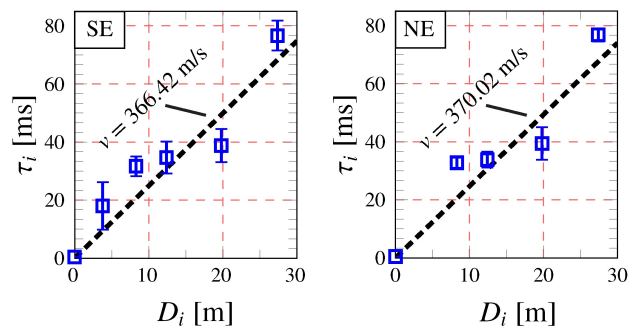

Figure 6. Travel time at different floors versus distance to the roof. The velocity is estimated as the global velocity of the waves crossing the whole structure for the stacked waveforms over the first 48 hours. The error bars denote the standard deviations of the travel times obtained for every 30-min long records (f_s=200 Hz).
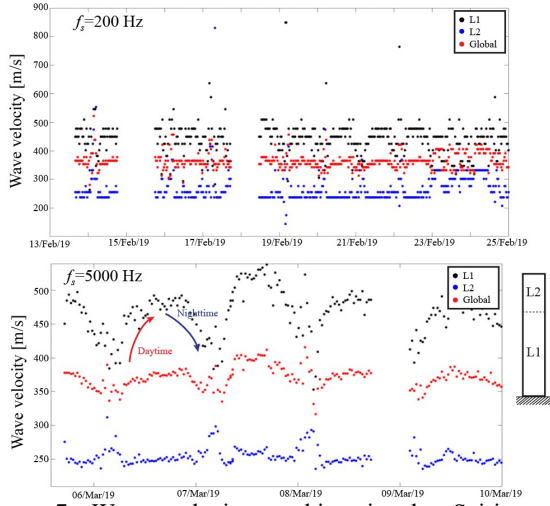
Figure 7. Wave velocity tracking in the Sciri tower considering two layers, L1 (9.3 m<z<28.4 m), and L2 (28.4 m<z<36.7 m), and the whole tower (9.3 m<z<36.7 m), with sampling frequencies of f_s=200 Hz and 5000 Hz.

layer, where thermal expansion is more constrained and the heterogeneity degree of the material is larger.

4 CASE STUDY II: CONSOLI PALACE

The Consoli Palace is the most conspicuous monument of the historical centre of Gubbio in Italy (Fig. 8). The palace was built between 1332 and 1349 to house the official courts of the Free Comune of Gubbio and, since 1901, the palace has hosted the Civic Museum. The palace is 60 m high and features a rectangular plan of about 40 × 20 m. A peculiar aspect of its structure is its foundation which, due to the steep slope of the site, is placed on two levels with a drop of approximately 10 m.

In order to complement a previous experience on the modal identification of the palace, the results of an AVT conducted on May 4th 2017 by Kita and co-authors (Kita et al. 2019) have been used here to identify the propagating waves in the palace. Eleven uni-axial accelerometers model PCB 393B12 were used in the test, although only the recordings of nine of them have been used in this work as sketched in Fig. 8. These sensors were deployed on the three main floors of the palace at heights of 4.64, 18.89 and 29.77 m. Ambient vibration data were collected in six separate 30 min long files at a sampling frequency of 1652 Hz using a data acquisition system model NI CompactDAQ-9132. For specific information on the results of the OMA identification, readers can refer to reference (Kita et al. 2019).
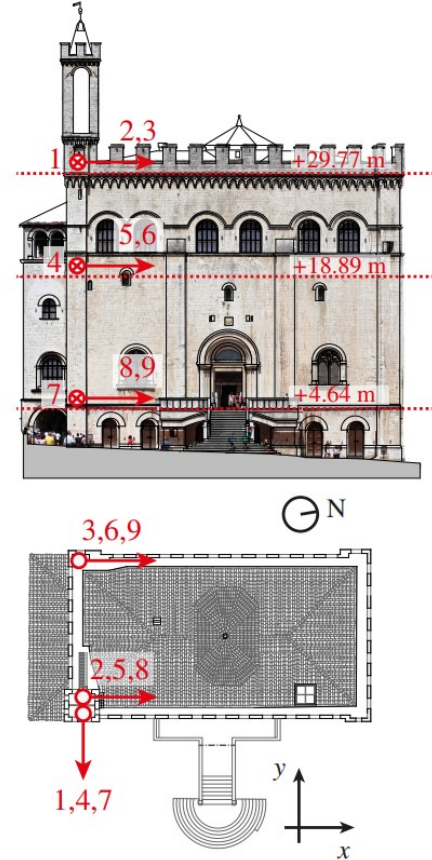

Figure 8. Sketch of the structural monitoring system deployed in the Consoli Palace.

A convergence analysis of the deconvolved waveforms for increasing time lengths is conducted in Fig. 9 based upon the root-mean-square misfit proposed by (Prieto et al. 2010):

$$\text{Misfit}(z,h) = \sqrt{\frac{\int_{t_a}^{t_b}\left[D_T(z,t)-D_{all}(z,t)\right]^2 \mathrm{d}t}{\int_{t_a}^{t_b}\left[D_{all}(z,t)\right]^2 \mathrm{d}t}}, \quad (1)$$

where t_a and t_b define the time interval used to compute the misfit (-1.5 s and 1.5 s in this study), T is the stacking duration, and D_T (z,t) and D_{all} (z,t) are the deconvolved IRFs at height z stacked over the time period T and the entire data set, respectively. In the analysis, time windows of different duration with 50% overlap have been considered, and stacked along the complete duration of the test (3 hours). It is noted in this figure that longer time windows lead to faster convergence rates. Moreover, it is observed in all the cases that the misfit decreases for an increasing number of stacked windows. Time windows of 10 minutes reach a misfit of 10% for around 35 windows, which is assumed accurate enough for the aim of the subsequent analyses.
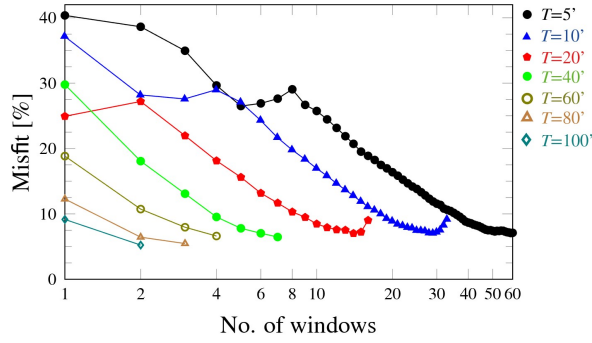
Figure 9. Convergence test of ambient noise interferometry in the *y*-direction (channels 1,4,7) of the Consoli Palace in terms of rms misfit, considering a sampling frequency of f_s = 200 Hz and band-pass filtered waveforms with cut-off frequencies of 2-9 Hz.
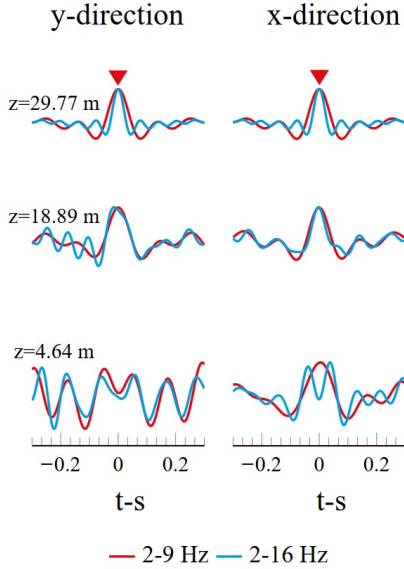

Figure 10. Band-pass filtered IRFs in the Consoli Palace considering 2-9 Hz and 2-16 Hz frequency bands, and stacked considering time windows of 10 minutes with 50% overlap (f_s = 100 Hz).

Table 2. Identified global wave delays τ and velocities v in the Consoli Palace (windows of 10 min with 50% overlap, f_s = 100 Hz).

	y-direction, channels 1, 4, 7		*x*-direction, channels 3, 6, 9	
	2-9 Hz	2-16 Hz	2-9 Hz	2-16 Hz
τ [ms]	50	60	-	40
v [m/s]	502.6	418.8	-	628.3

Figure 10 shows the stacked waveforms in the *y*-direction (channels 1, 4, and 7) and the *x*-direction (channels 3, 6, and 9) considering a sampling frequency f_s = 100 Hz. In addition, two different frequency bands are considered, namely 2-9 Hz and 2-16 Hz. It is noted in this figure that travelling pulses in the frequency band 2-9 Hz can be only identified in the *y*-direction. Conversely, travelling pulses can be identified in

both directions when the wider frequency band 2-16 Hz is considered. This is due to the limited separation between the sensors and the fact that wider frequency bands yield propagating pulses narrower in time (see Ebrahimian et al. 2014), in such a way that the identification of two independent pulses can be more easily conducted. It can be visually noted that waves travel faster in the *x*-direction and, as a result, travelling pulses can be only identified in the second frequency band. Finally, Table 2 reports the global wave delays τ and velocities v obtained by peak-picking analysis in the *y*- and *x*-directions of the Consoli Palace. Note that, owing to the larger stiffness of the building in the *x*-direction, the velocity of the waves is higher in this direction.

5   CASE STUDY III: BELL-TOWER OF THE BASILICA OF SAN PIETRO

The last case study is the bell-tower of the Basilica of San Pietro located in the city of Perugia, Italy. The construction of the Basilica dates back to 996, although the bell-tower was not erected until the 13th century. Three main structural portions can be distinguished in the tower, namely a shaft, a belfry, and a cusp. The shaft stands 26 m high and has a dodecagonal cross-section. The belfry extends up to a height of 40.8 m and has a hexagonal cross-section and, finally, the brick masonry cusp completes the tower with a total height of 61.4 m. The bell-tower experienced moderate damage during the 2016 Central Italy seismic sequence as reported by Ubertini and co-authors (Ubertini et al. 2018). The seismic sequence consisted of the Accumoli Mw 6.0 earthquake of August 24th, followed by the Ussita Mw 5.9 and Norcia Mw 6.5 earthquakes of October 26th and 30th, respectively, and the presence of damage could be inferred from permanent variations in the resonant frequencies of the tower.

In this work, two AVTs, conducted before and after the 2016 Central Italy seismic sequence, have been used to assess the earthquake-induced damage through OMA and ANDI. The first AVT was carried out in February 2015 by using five high-sensitivity (10 V/g) accelerometers, model PCB 393B12. As sketched in Fig. 11 (a), the sensors were placed at two different levels, namely z = 41 m and z = 25 m, and the acceleration records were collected through a DAQ system located at z = 21 m. On the other

hand, the second AVT was carried out in May 2017 and consisted of twelve accelerometers model PCB 393B12 deployed at four different levels as shown in Fig. 11 (b), namely $z = 41$ m, $z = 29.1$ m, $z = 26.8$ m, and $z = 12.5$ m, as well as a DAQ system located at $z = 21$ m. In both cases, ambient vibrations were recorded for 30 minutes at a sampling frequency of 100 Hz.

Table 3 presents the comparison between the modal features extracted by means of COV-SSI. A total of seven modes have been identified in the AVT of May 2017 with resonant frequencies up to 10 Hz, and the mode shapes are depicted in Fig. 12. These include first (Fx1, Fy1), second (Fx2, Fy2), and third flexural modes (Fx3, Fy3), with x and y denoting the prevailing direction of the motion, as well as a torsional mode T1. The same modes have been identified in the AVT of February 2015, except for the mode Fx3, what can be ascribed to limitations in the monitoring of the x-direction of the tower only by channels 1 and 4. The comparison between the modal features has been conducted in terms of MAC values (Modal Assurance Criterion), and relative differences between resonant frequencies f_i. It is noted that, since the relative differences in terms of resonant frequencies do not show a clear pattern, damage cannot be directly inferred from frequency shifts. This is due to the dependence of the resonant frequencies upon environmental effects as reported by Ubertini and co-authors (Ubertini et al. 2018). In that work, those authors showed that the earthquake-induced frequency shifts are masked by daily temperature fluctuations. It was thus imperative to detrend the natural frequencies identified by long-term monitoring considering environmental effects, and so identify damage-induced permanent variations through a novelty analysis, which cannot be done by single AVTs and OMA.

Finally, since mode shapes are presumably less sensitive to temperature, the comparison of MAC values can give more insight into the presence of damage. It is noted in Table 3 that the MAC values for the modes Fx1, Fy1 and T1 are close to one, that is to say, no significant differences are found before and after the seismic sequence. Conversely, lower MAC values are found for higher order modes in which local stiffness effects play a more relevant role. Therefore, it is concluded that these results may evidence the presence of damage, although its

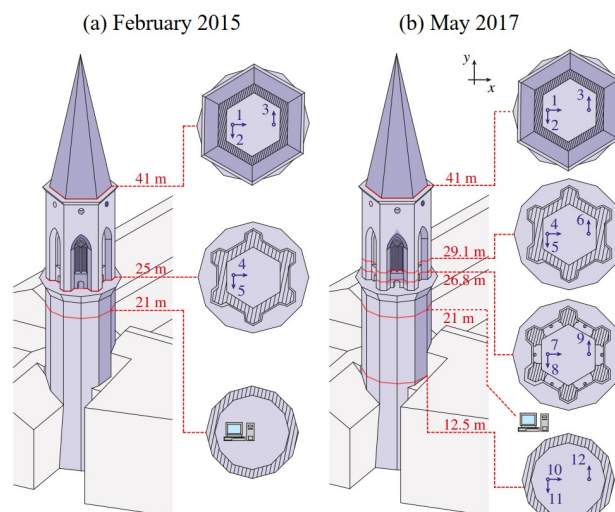localization would require the inverse calibration of a numerical model.

Figure 11. Sketch of the AVT conducted in February 2015 (a), May 2017 (b), on the masonry bell-tower of the Basilica of San Pietro.

Figure 13 shows the wave velocities obtained by peak-picking analysis of low-pass filtered IRFs versus the cut-off frequency. Given the larger sensor density in the AVT of May 2017, the wave velocities are obtained in this case between the heights 12-41 m (global velocity accounting for both the shaft and belfry areas, channels 1 and 10) and 26.8-41 m (local velocity isolating the belfry area, channels 1 and 7), denoted with asterisk and double asterisk in Fig. 13, respectively. It is clearly observed that the seismic sequence produced reductions in the wave velocities or, in other words, stiffness losses due to earthquake-induced damages. In particular, relative reductions of 5.0%, 10.1% and 9.4% are obtained in terms of global velocity for cut-off frequencies of 11 Hz, 15 Hz and 20 Hz, respectively. Larger reductions of 19.9%, 16.3% and 21.7% are obtained in terms of local velocity in the area of the belfry for cut-off frequencies of 11 Hz, 15 Hz and 20 Hz, respectively. These variations are consistent with the results reported by Ubertini and co-authors (Ubertini et al. 2018), who found cumulated decays in the temperature-detrended resonant frequencies of 7.6%, 5.7%, 10.8%, 5.1% and 4.0% for the modes Fx1, Fy1, T1, Fy2 and Fy3, respectively. The larger reductions in wave velocities found in the area of the belfry also confirm the concentration of earthquake-induced cracks in this region reported by the numerical simulations of Cavalagli and co-

authors (Cavalagli et al. 2018). Therefore, these results demonstrate the applicability of ANDI for damage detection, localization and, to some extent, quantification in masonry structures.

6 CONCLUSIONS

This paper has presented the synergistic application of OMA and ANDI for structural and damage identification in historic structures, and the application experience on three Italian masonry structures has been presented to demonstrate its effectiveness. These include the Sciri Tower in Perugia, the Consoli Palace in Gubbio, and the bell-tower of the Basilica of San Pietro in Perugia. Firstly, continuous full system identification has been conducted through OMA and ANDI in the Sciti Tower. The results have demonstrated that a high sampling frequency is required to identify the temperature fluctuations of the velocity of the shear S-waves travelling in the tower. Afterwards, the Consoli Palace has been presented as a case study of a complex masonry building with limited distance between the sensors. In this case, the study has focused on the robustness of the identification of wave velocities through peak-picking analysis for increasing stacking time windows. Finally, the bell-tower of the Basilica of San Pietro has been presented as an illustrative case study of damage identification. To do so, two different AVTs conducted in February 2015 and May 2017, that is before and after the 2016 Central Italy seismic sequence, have been used. The results have demonstrated that OMA is primarily effective for detecting the presence of damage, and that the use of ANDI offers superior capabilities for damage identification, including localization and quantification.
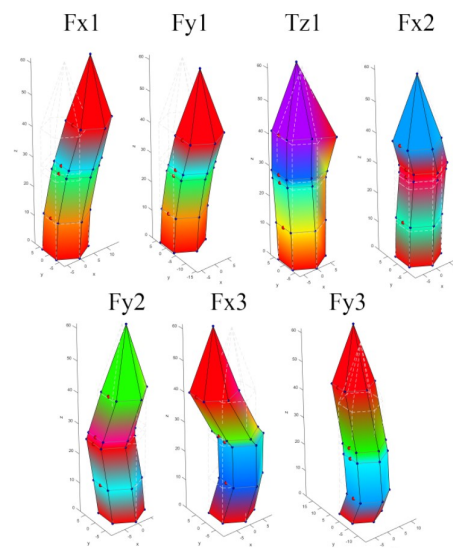
Figure 12. Experimentally identified mode shapes of the Basilica of San Pietro by SSI from the AVT of May 2017.

Table 3. Comparison of the experimentally identified modal features of the masonry bell-tower of the Basilica of San Pietro by COV-SSI from AVTs conducted in February 2015 and May 2017.

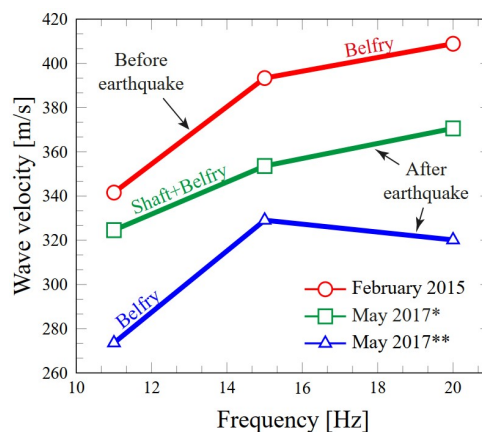| Mode	Feb. 2015 f_i [Hz]	May 2017 f_i [Hz]	MAC	$100\dfrac{\Delta f_i}{f_i|_{2015}}$
Fx1	1.45	1.46	0.99	-31.9
Fy1	1.52	1.53	0.99	-32.2
T1	4.35	4.20	0.99	-44.6
Fx2	4.57	4.48	0.75	-48.5
Fy2	4.89	5.00	0.72	-31.3
Fx3	-	7.12	-	-
Fy3	7.24	7.22	0.79	-18.3

Figure 13. Wave velocities versus cut-off frequency obtained by peak-picking analysis of low-pass filtered IRFs computed on the basis of the AVTs conducted in February 2015 and May 2017 in the bell-tower of the Basilica of San Pietro (30 minutes, f_s=100 Hz).

REFERENCES

Cavalagli, N., Comanducci, G., Ubertini, F., 2018. Earthquake-induced damage detection in a monumental masonry bell-tower using long-term dynamic monitoring data, *Journal of Earthquake Engineering*, **22**, 96–119.

Ebrahimian, M., Rahmani, M., Todorovska, M. I., 2014. Nonparametric estimation of wave dispersion in high-rise buildings by seismic interferometry, *Earthquake Engineering & Structural Dynamics*, **43**, 2361–2375.

Kita, A., Cavalagli, N., Ubertini, F., 2019. Temperature effects on static and dynamic behavior of Consoli Palace in Gubbio, Italy, *Mechanical Systems and Signal Processing*, 120, 180–202.

Masciotta, M. G., Ramos, L. F., Lourenço, P. B., 2017. The importance of structural monitoring as a diagnosis and control tool in the restoration process of heritage structures: a case study in Portugal, *Journal of Cultural Heritage*, **27**, 36–47.

Nakata, N., Snieder, R., 2013. Monitoring a building using deconvolution interferometry. II: Ambient-vibration analysis, *Bulletin of the Seismological Society of America*, **104**, 204–213.

Prieto, G. A., Lawrence, J. F., Chung, A. I., Kohler, M. D., 2010. Impulse response of civil structures from ambient noise analysis, *Bulletin of the Seismological Society of America*, 2322–2328.

Șafak, E., 1999. Wave-propagation formulation of seismic response of multistory buildings, *Journal of Structural Engineering*, **125**, 426–437.

Snieder, R., Șafak, E., 2006. Extracting the building response using seismic interferometry: Theory and application to the Millikan Library in Pasadena, California, *Bulletin of the Seismological Society of America*, **96**, 586–598.

Todorovska, M. I., Trifunac, M. D., 2008. Earthquake damage detection in the Imperial County Services Building III: analysis of wave travel times via impulse response functions, *Soil Dynamics and Earthquake Engineering*, **28**, 387–404.

Ubertini, F., Cavalagli, N., Kita, A., Comanducci, G., 2018. Assessment of a monumental masonry bell-tower after 2016 Central Italy seismic sequence by long-term SHM, *Bulletin of Earthquake Engineering*, **16**, 775–801.